

PAPER

2-Dimensional Imaging of Human Bodies with UWB Radar Using Approximately Uniform Walking Motion along a Straight Line with the SEABED Algorithm

Takuya SAKAMOTO^{†a)}, *Member* and Toru SATO[†], *Fellow*

SUMMARY UWB (Ultra Wide-Band) pulse radar is a promising candidate for surveillance systems designed to prevent crimes and terror-related activities. The high-speed SEABED (Shape Estimation Algorithm based on BST and Extraction of Directly scattered waves) imaging algorithm, is used in the application of UWB pulse radar in fields that require real-time operations. The SEABED algorithm assumes that omni-directional antennas are scanned to observe the scattered electric field in each location. However, for surveillance systems, antenna scanning is impractical because it restricts the setting places of the devices. In this paper, movement of a body is used to replace antenna scanning. The instantaneous velocity of any given motion is an unknown variable that changes as a function of time. A pair of antennas is used to analyze delay time to estimate the unknown motion. We propose a new algorithm to estimate the shape of a human body using data obtained from a human body passing stationary antennas.

key words: UWB radar, SEABED algorithm, walking motion, surveillance system

1. Introduction

Radar imaging is a promising candidate for surveillance systems used, for example, to prevent crimes and terror-related activities. Radar can be installed in private areas where cameras cannot be used because of privacy concerns. For example, it is not appropriate to install cameras in passageways in restrooms, locker rooms, or shower areas, which can create a security hole in a surveillance system. It is possible to obtain the shapes of bodies without their surface texture using UWB pulse radar, providing surveillance of activities while avoiding many privacy concerns.

Lin and Ling [1], [2] propose a low-complexity radar system for frontal imaging of moving humans. They use a three-element receiving array and a transmitter with a CW (Continuous Wave) signal. They experimentally imaged moving body to construct a frontal view of a human. Their technique, however, is based on the assumption that different body parts give rise to different Doppler frequencies. It is difficult to meet this condition in practice, which leads to inaccurate imaging.

UWB (Ultra Wide-Band) pulse radar is an alternative candidate. It is reliable as a surveillance system because it does not depend on Doppler frequencies. A variety of algo-

rithms have been proposed to estimate target shape with observed UWB radar data [3]–[5]. However, most of these are based on iterative procedures, which makes the calculation time too long for application in surveillance systems. We have developed SEABED, a high-speed imaging algorithm [6]–[8], to enable the use of UWB pulse radar in areas that require realtime operations, such as automobiles, robotics, and surveillance. Surveillance systems need to finish processing signals to obtain the image within a short time to prove useful. The SEABED algorithm is indispensable in this task. The SEABED algorithm is based on a reversible BST (Boundary Scattering Transform) between the target shape and the received data and does not require iterative calculations as is the case for many other algorithms used in this kind of application, such as, the synthetic aperture method or the domain integral equation method [9].

The SEABED algorithm assumes omni-directional antennas are scanned to observe the scattered electric field at each location. In robotics, robot motion can be easily made to match the scanning process. However, for surveillance systems the motion of detection devices is limited because they are usually installed on walls or other fixed observation points. For this reason antenna scanning is not realistic for surveillance systems. In this paper, walking motion is used to replace the need for scanning antennas. Data is instead gathered from signals from various antennas with differing relative positions to the subject. This data is approximately equal to the data obtained by scanning of antennas except in one key facet: the instantaneous velocity of any given walking motion is an unknown variable which changes as a function of time. We propose a new algorithm that solves this problem and uses the available data to estimate the shape of a human body.

2. System Model

For the purposes of this paper it is assumed that the radar is installed on walls in passageways as in Fig. 1. People tend to walk approximately uniformly in passageways in subways and airports, compared to other places such as outside in the open. The motion is not, however, completely uniform; this non-uniformity can be seen as an unknown function.

For simplicity, we deal with a 2-dimensional problem in this paper, where the objective is to estimate the shape of the cross-section of human bodies. We use a pair of omni-

Manuscript received February 21, 2008.

Manuscript revised July 1, 2008.

[†]The authors are with the Department of Communications and Computer Engineering, Graduate School of Informatics, Kyoto University, Kyoto-shi, 606-8501 Japan.

a) E-mail: t-sakamo@i.kyoto-u.ac.jp

DOI: 10.1093/ietcom/e91-b.11.3695

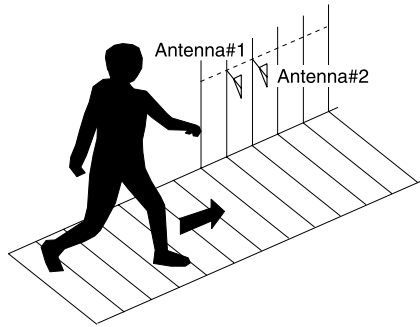


Fig. 1 Antenna arrangement for imaging human bodies.

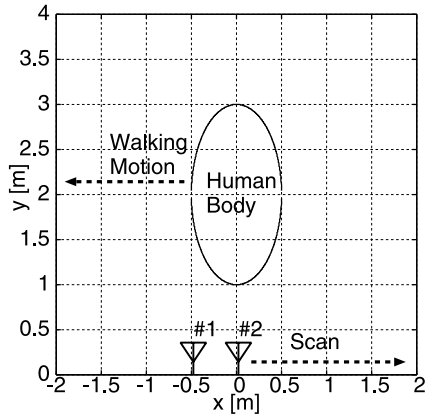


Fig. 2 2-dimensional system model.

directional antennas at a set distance; X_0 . We measure the range between the scattering center and each receiving antenna. The measurement is independent of the position of the other antenna in the system, which means that we assume a dual monostatic radar system instead of a bistatic radar system. This dual monostatic radar system is created by introducing a spectrum spreading modulation with two different codes assigned to the antennas. The interference between these signals can be reduced to zero by adopting orthogonal codes. In this paper, we assume the direction of the walking motion is parallel to the baseline of the antennas and the speed is an unknown function of time. Figure 2 shows the 2-dimensional system model dealt with in this paper, where $X_0 = 0.5\lambda$ is assumed for the center wavelength λ .

Only the position of the antennas relative to the target object is considered, inverting the problem to be solved to one of estimating the unknown motion of the antennas scanning a ‘stationary’ target object. The problem is viewed in this way in the following discussions purely for simplicity.

3. The SEABED Algorithm

A fast BST-based radar imaging algorithm has been developed in previous works [6], [9]. The algorithm is named SEABED: Shape Estimation Algorithm based on BST and extraction of directly scattered waves. The algorithm uses

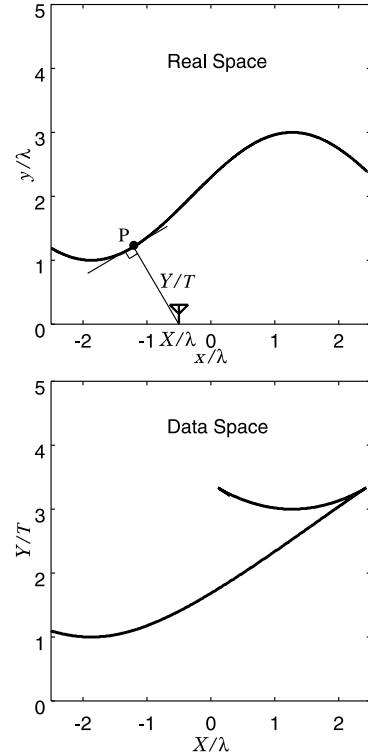


Fig. 3 An example of a target shape and a quasi wavefront.

the existence of a reversible BST between target shapes and pulse delays. SEABED has the advantage of direct estimation of target boundaries using the inverse transform, and a mathematically complete solution for the inverse problem has been shown. It is assumed that each target has a uniform complex permittivity, and is surrounded by a clear boundary. It is also assumed that the propagation speed is constant and known.

The upper part of Fig. 3 shows an example of a target shape, where x, y and X are normalized by the center wavelength λ , and the delay time Y is normalized by the center period $T = \lambda/c$ with the speed of light c . A strong scatterer is received from point P in the figure. The distance Y between the point P and the antenna $(X, 0)$ is easily obtained from UWB radar. The relationship between X and Y is shown in the lower part of Fig. 3. We call this curve a ‘quasi-wavefront.’ The BST is expressed as

$$X = x + y \frac{dy}{dx}, \tag{1}$$

$$Y = y \sqrt{1 + \left(\frac{dy}{dx}\right)^2}, \tag{2}$$

where (X, Y) is a point on a quasi-wavefront, and (x, y) is a point on the target boundary [6]. As stated above the inverse transform of the BST is given by

$$x = X - Y \frac{dY}{dX}, \tag{3}$$

$$y = Y \sqrt{1 - \left(\frac{dY}{dX}\right)^2}, \quad (4)$$

where we assume $|dY/dX| \leq 1$. This condition is required because y should be a real number and can be used as a clue to estimate quasi-wavefronts from the received signals. We call the transforms in Eqs. (3) and (4) Inverse Boundary Scattering Transforms (IBST's).

First, quasi-wavefronts are extracted from the received signals $s(X, Y)$ using the SEABED algorithm. These wavefronts are extracted to satisfy the conditions $ds(X, Y)/dY = 0$ and $|dY/dX| \leq 1$. Next, quasi-wavefronts with a large evaluation value, calculated by summing the signal power along the estimated quasi-wavefront, are selected. Lastly, the IBST is applied to the quasi-wavefronts to obtain the final image.

4. Observed Data with Unknown Scanning Speed

In the SEABED algorithm, the IBST is applied to the quasi-wavefront $Y(X)$ to obtain the estimated shape (x, y) . The quasi-wavefront is the relationship between the antenna position X and the delay time Y . It should be noted that the antenna position is not known; the position X must, therefore, be estimated to obtain the quasi-wavefront.

The positions of the antennas 1 and 2 at time t are $(X(t), 0)$ and $(X(t) + X_0, 0)$, respectively because the distance between the antennas is X_0 . Under this assumption, the delay times observed with the pair of antennas are

$$Y_1(t) = Y(X(t)), \quad (5)$$

and

$$Y_2(t) = Y(X(t) + X_0) \quad (6)$$

as functions of time t with the quasi-wavefront $Y(X)$. It is important to note that these functions are composite functions of $X(t)$ and $Y(X)$. The equations $Y_1(t)$ and $Y_2(t)$ are required to estimate the original functions $X(t)$ and $Y(X)$. If $Y(X)$ is correctly estimated, it is easy to estimate the target shape using the IBST as described in the previous section.

5. Proposed Algorithm

We propose an algorithm to readily estimate $X(t)$ and $Y(X)$. First, the pair of times t_1 and t_2 that satisfies $Y_1(t_1) = Y_2(t_2)$ is calculated. It then follows that the antennas are located at the same position at t_1 and t_2 , respectively. The t_1, t_2 pair is sequentially calculated, and the continuous function $\tau(t)$, that satisfies

$$Y(X(\tau(t))) = Y(X(t) + X_0), \quad (7)$$

is estimated. This, in turn, is equal to the condition $t_1 = \tau(t_2)$. To obtain the function $\tau(t)$, we roughly match the delay times $Y_1(t)$ and $Y_2(t)$ with the average time difference t_0 . Here, t_0 is a constant and approximately satisfies

$$Y_1(t + t_0) \simeq Y_2(t), \quad (8)$$

which is determined using the peak time of the cross-correlation function of $Y_1(t)$ and $Y_2(t)$ as

$$t_0 = \operatorname{argmax}_{t_0} \left| \int Y_1(t + t_0) Y_2(t) dt \right|^2. \quad (9)$$

Next, the minute adjustment function $\Delta\tau(t)$ must be solved to satisfy

$$Y_1(t + t_0 + \Delta\tau(t)) = Y_2(t), \quad (10)$$

where $\Delta\tau(t)$ is estimated by a simple linear search. If multiple candidates that satisfy the condition in Eq. (10) are found for $\Delta\tau(t)$, we adopt the one that has the minimum absolute value $|\Delta\tau(t)|$ among them. Then, the function $\tau(t) = t + t_0 + \Delta\tau(t)$ is obtained.

The function $\tau(t)$ approximately satisfies $X(\tau(t)) = X(t) + X_0$. The equation:

$$\frac{X(\tau(t)) - X(t)}{\tau(t) - t} = \frac{X_0}{\tau(t) - t} \quad (11)$$

can, therefore, be easily derived. If the time difference $|\tau(t) - t|$ is small, the left-hand side of Eq. (11) can be approximated as the derivative dX/dt . However, if $|\tau(t) - t|$ is not sufficiently small, the approximation has a time offset.

Interestingly, we can also derive another equation:

$$\frac{X(t) - X(\tau^{-1}(t))}{t - \tau^{-1}(t)} = \frac{X_0}{t - \tau^{-1}(t)}. \quad (12)$$

Here, the inverse function $\tau^{-1}(t)$ naturally satisfies $t_2 = \tau^{-1}(t_1)$, similarly to $t_1 = \tau(t_2)$. If the left-hand side of the equation is approximated as the derivative dX/dt , Eq. (12) also has an offset. The following approximation can be adopted as a compromise:

$$\frac{dX}{dt} \simeq \frac{X(\tau(t)) - X(\tau^{-1}(t))}{\tau(t) - \tau^{-1}(t)} = \frac{2X_0}{\tau(t) - \tau^{-1}(t)}. \quad (13)$$

This approximation is similar to the concept of centered difference. The right-hand side of Eq. (13) is calculated with the estimated $\tau(t)$. Then, an integration is performed to estimate $X(t)$ as

$$X(t) \simeq \int \frac{2X_0}{\tau(t) - \tau^{-1}(t)} dt + C, \quad (14)$$

where C is an integral constant. This constant C cannot be determined with observed signals. However, we are not concerned with the constant C here because it only influences position, not shape.

Finally, the quasi-wavefront $Y(X)$ is calculated using the estimated $X(t)$ with Eq. (5). The target shape can be obtained by applying the IBST to the estimated quasi-wavefront.

6. Application of the Proposed Algorithm

This section discusses examples of practical applications of the proposed algorithm. It is assumed that the true target shape is an ellipse as shown in Fig. 2. The distance between the antennas is set to 0.5λ . The speed of the walking motion is assumed to change according to the solid line in Fig. 4 with an average speed of 1m/s, as shown by the dashed line in this figure.

Figure 5 shows the estimated range data for the antennas. The sampling interval is assumed to be 5 msec. If the walking motion is uniform with a known velocity, it is possible to estimate the target shape by applying an IBST. First, the IBST is applied to the data in Fig. 5 assuming uniform motion at a speed of 1 m/s to obtain the target shape in Fig. 6. The estimated shape has a large error except around $x = 0$. This is because the assumed speed is equal to the average motion at $t = 0$ and $x = 0$ as in Fig. 4. The conventional SEABED algorithm assumes antenna scanning motion is uniform, which causes this kind of large error in the estimated image.

Interferometric techniques are often used to estimate target motion in this field [1]. These techniques, however, assume that the scattering center is fixed. If this assumption

is satisfied, the motion $x_p(t)$ can be estimated as

$$x_p(t) = \frac{Y_1(t)^2 - Y_2(t)^2 + X_0^2}{2X_0}, \tag{15}$$

which is calculated as the dashed line in Fig. 7; the true motion is shown as a solid line. Here, the estimated motion is close to the true motion when compared to the approximation using uniform motion. However, the estimation error is still not negligible, because the assumption that the scattering center is fixed is unrealistic, and results in the scattering center moving relative to the scanning antenna. The actual model for a moving scattering center and the approximation model for a fixed scattering center are shown in Fig. 8. The models in this figure illustrate that this interferometric approximation is not valid for our assumed system.

Figure 9 shows the estimated motion produced by the proposed algorithm. The estimation error is smaller than that of conventional interferometry. There are errors at the left and right ends. This is because $Y_1(t)$ and $Y_2(t)$ are truncated at both the ends as shown in Fig. 5, and cannot match for any value of $\tau(t)$ assumed. Figure 10 shows the target shape estimated with the proposed algorithm. Here, the images estimated at the left and right ends are removed because of large errors in these areas caused by motion estimation.

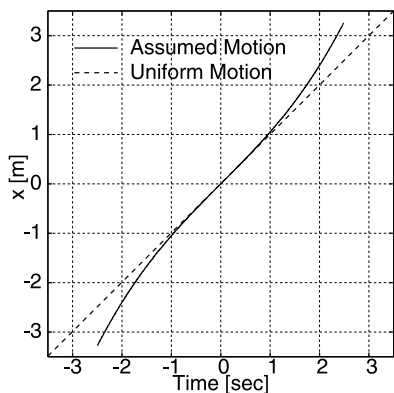


Fig. 4 Assumed relative position and uniform motion in the conventional SEABED algorithm.

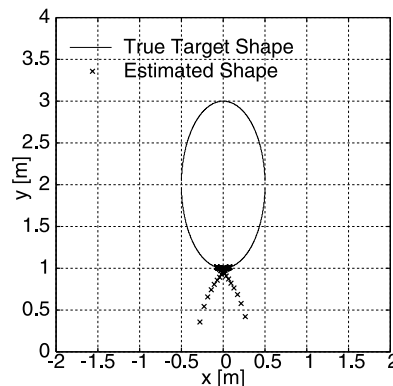


Fig. 6 Estimated target shape using the conventional SEABED algorithm.

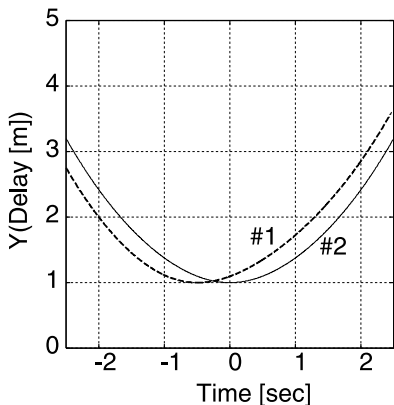


Fig. 5 Observed range vs. time.

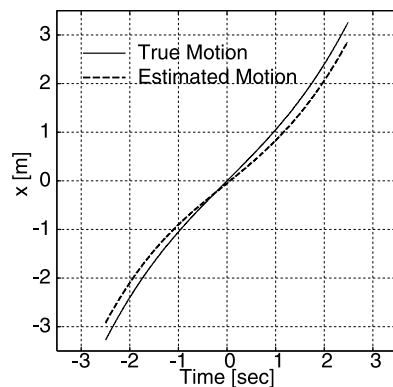


Fig. 7 Estimated relative position by interferometric measurement for a point target.

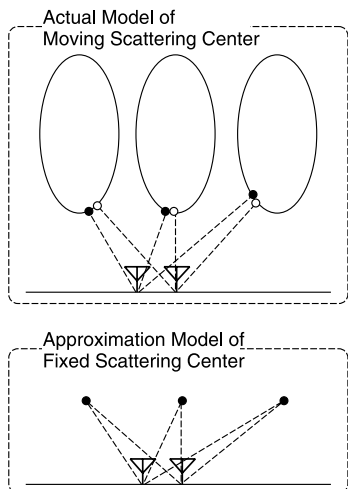


Fig. 8 Actual and approximation models of scattering center.

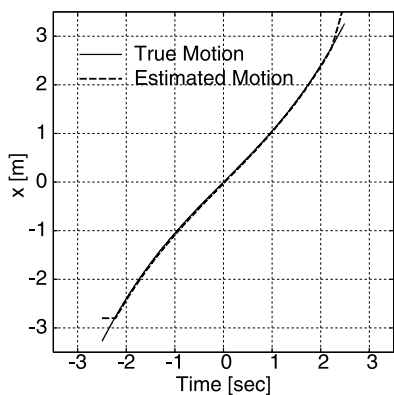


Fig. 9 Estimated relative position using the proposed algorithm.

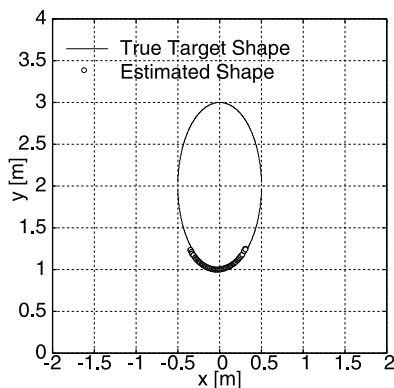


Fig. 10 Target shape estimated with the proposed algorithm.

The shape is accurately estimated because the error in the estimated walking motion $X(t)$ is small enough for the imaging process using the proposed algorithm.

7. Performance Evaluation of the Proposed Method Using a Realistic Model

7.1 Measurement of Walking Motion

In the previous section, we investigated the performance of the proposed method with a simple model of walking motion. Real walking motion should be used to study the feasibility of the method because the walking motion model is critical for the motion estimation process. To measure real walking motion, we use a video camera in a test site as in Fig. 11, where the walking course is a straight line and the distance between the camera and course is set to 6.5 m. This distance was determined empirically, and influences the measured width and the accuracy of estimated motion. Figure 12 shows a picture of the site used for measurement and some snapshots of a walking man are displayed. The top of the head is detected with simple image processing.

1. The background image is recorded as a reference image.
2. A walking human is recorded as a video footage with a camera.
3. The reference image is subtracted from the recorded images.
4. The image is binarized.
5. The boundary of the image is enhanced with a Laplacian filter.
6. A Gaussian LPF (Low-Pass Filter) is applied for smoothing.
7. The maximum point is detected as the top of a head.

In this experiment, one examinee was instructed to walk naturally straight forward from the left of the area depicted to the right.

Data obtained from the walking motion in this experimental setup is shown in Fig. 13. The time origin $t = 0$ is defined to satisfy $X(0) = 0$ here. This figure shows that the measured walking motion is close to uniform. A straight line $x_s(t) = v_0t + x_0$ is determined by LMS (Least Mean Square) fitting, and is subtracted from the real walking motion. The remaining, minute, fluctuation component $\Delta x(t) = x(t) - x_s(t)$ is shown as the dashed line in Fig. 14. Because this fluctuation component contains quantization noise, an LPF is applied and the result $\Delta x_s(t)$ is shown as the solid line in Fig. 14. The period of the fluctuation is about 0.5sec and is almost synchronized with the walking steps.

7.2 Application of the Proposed Method to Experimental Data

Real walking motion is depicted in Fig. 14. We investigated the performance of the proposed method using this experimental data. The approximated solid line in Fig. 14 and the determined regression line are used as a realistic walking-motion model: $x_s(t) + \Delta x_s(t)$. We assume the same parameters as used in the numerical simulations for the antenna

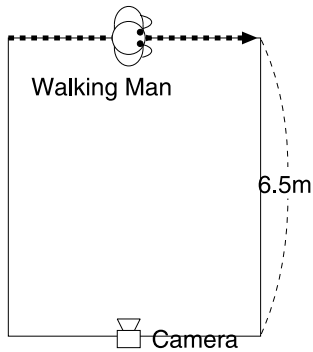


Fig. 11 Camera arrangement for measurement of walking motion.



Fig. 12 Experimental site for measurement of walking motion.

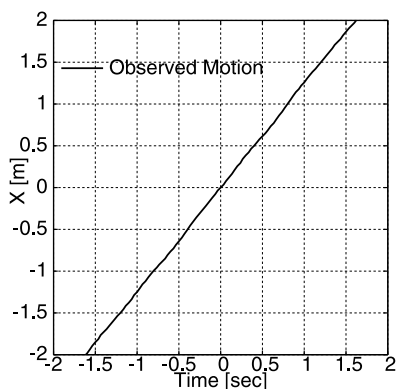


Fig. 13 Measured walking motion.

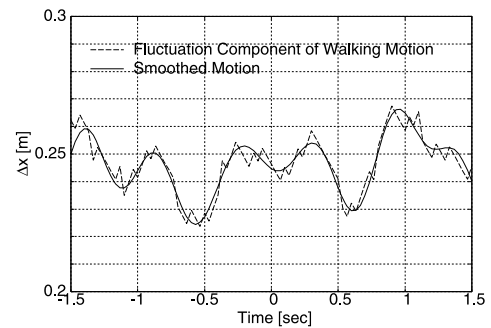


Fig. 14 Fluctuation component of real walking motion.

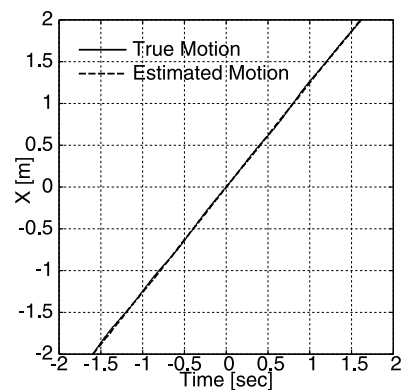


Fig. 15 Estimated walking motion with experimental data.

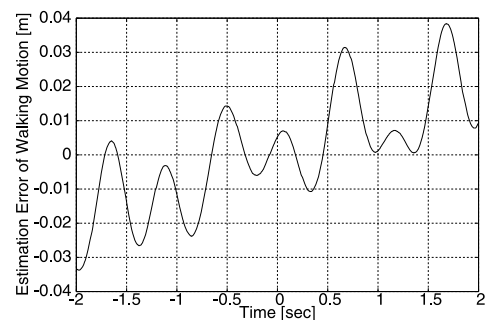


Fig. 16 Estimation error of walking motion with experimental data.

interval and human body shape.

It was confirmed that the estimated walking motion is substantially accurate as shown in Fig. 15. In this figure, the solid and dashed lines show the estimated and true motion, respectively. The estimation error is shown in Fig. 16. This figure shows that the estimation error is a few centimeters at most. Figure 17 shows the estimated target shape for the realistic walking model. Although the estimated image has some error points, the entire target shape is estimated quite accurately by the proposed method. In the figure, the points with large error are caused by the estimation error of walking motion as in Fig. 16. This motion error is translated to the error in quasi-wavefronts. The IBST for Eqs. (3) and

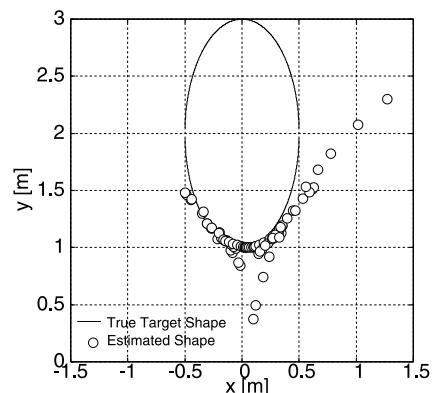


Fig. 17 Estimated target shape with experimental data.

(4) contain derivative operations, which makes the image sensitive to random components in the quasi-wavefronts. This characteristic amplifies the relatively small motion error leading to the large error in the image.

8. Discussion

8.1 Walking Motion Model

The application examples shown above assumed approximately uniform motions, whose validity was confirmed by the experimental observation. Here, we discuss some aspects of the motion model.

The estimation accuracy of the proposed algorithm degrades when applied to a walking motion with high acceleration. Here, we show an example of the results of the proposed algorithm for a motion with high acceleration. The solid line in Fig. 18 shows motion with higher acceleration than in Fig. 4. In this figure, the estimated motion is shown as the dashed line. The estimation accuracy is lower than the previous case in Fig. 9 because the approximation in Eq. (13) fails. This inaccuracy is accumulated and becomes large with the integration in Eq. (14), which is confirmed by the large error in the right part of the estimated motion for $t > 1.3$ sec in Fig. 18. The observed quasi-wavefronts are shown in Fig. 19, where we see the bottom of each quasi-wavefront is flat compared to that in Fig. 5 because the assumed motion here has low velocity around $t = 0$. These flat bottoms make it difficult to accurately determine $\tau(t)$, which is sensitive to random components in a noisy environment. The estimated image is shown in Fig. 20. In this figure, only a part of the target shape is estimated and there are points with large error caused by the error in the motion estimation process. If the acceleration increases, the estimation accuracy is severely degraded by these effects.

In the paper, we assume that a target moves along a straight line. When the motion contains a fluctuation perpendicular to the direction of travel, the estimated shape degrades because the IBST cannot be used for imaging because the IBST requires a straight scanning. Additionally, the motion estimation process becomes difficult because the

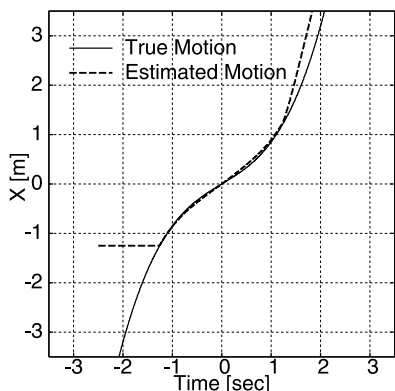


Fig. 18 Assumed motion with high acceleration and the corresponding estimated motion.

relationship between Eqs. (5) and (6) cannot be used. Resolving this is an important future task for the application of this method to real environments.

8.2 Target Size and Shape for the System Model

The target size above $(2\text{ m} \times 1\text{ m})$, is far larger than the human body. We adopted this target size as a worst case scenario. The imaging problem becomes difficult as the target size increases because scattering center movement is the main problem for imaging as explained in Fig. 8. Figure 21

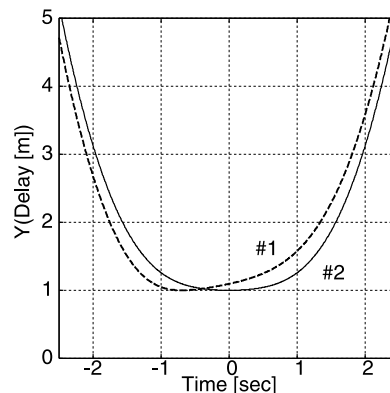


Fig. 19 Observed quasi-wavefronts for motion with high acceleration.

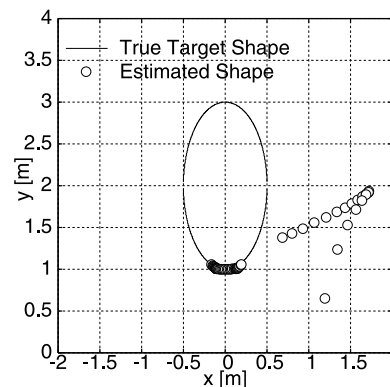


Fig. 20 Estimated image for motion with high acceleration.

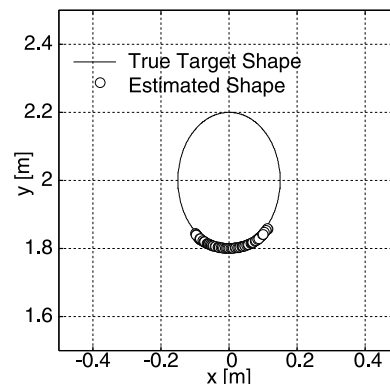


Fig. 21 Estimated target shape for target size $0.4\text{ m} \times 0.3\text{ m}$.

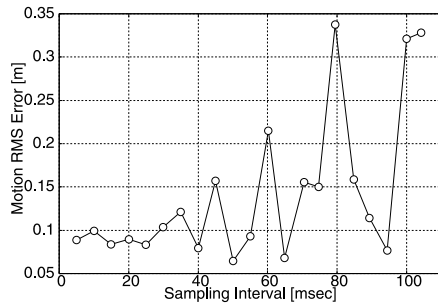


Fig. 22 Estimation accuracy of walking motion vs. the sampling interval of time.

shows the estimated image assuming all the same parameters as in Section 6 except for target size. The assumed target size is $0.4 \text{ m} \times 0.3 \text{ m}$, and this target shape is accurately estimated in this case.

As for the target shape, we assume a simple shape (an ellipse) in this paper. In reality clothes, bags and other items will influence the results of the proposed method. Firstly, they make the target shape complex, and the extraction process of quasi-wavefronts becomes difficult. We have developed an effective method for this kind of problem with complex-shaped targets in previous work [10]. Secondly, they make the reflection power small compared to the specular reflection model assumed in this manuscript. For signals with low S/N, another technique can be adopted to stabilize the image [11]. Finally, they make the walking motion complicated, for which our simple motion model cannot be used. Solving this problem is an important future task for this course of research.

8.3 Performance for Various Sampling Intervals

For the application examples of imaging in the previous sections, we assumed a sampling interval Δt to be 5 msec. The sampling interval influences the determination of $\tau(t)$ because the sampling of data $Y(t)$ corresponds to the quantization of $\tau(t)$. Figure 22 shows the relationship between the estimation RMS(Root-Mean-Square) error for walking motion and the sampling interval Δt , where we assume all the parameters are the same as in Sect. 6 except for Δt . In this figure, we see that the estimation error becomes large especially for $\Delta t > 30$ msec. Please note that this result is based on a walking motion model with about 1 m/sec as assumed throughout this paper. As the speed of a target motion increases, the sampling interval should be shortened. This means that the maximum speed, to which our method is applicable, depends on the sampling interval. It is, thus, important to determine the maximum sampling interval for any general walking motion model.

9. Conclusion

This paper discusses the applicability of UWB radar imaging to surveillance systems. We used walking motion to replace antenna scanning to observe the electric field in var-

ious positions, where walking motion is an unknown function of time. A new algorithm to estimate both walking motion and target shape was proposed. We approximated the derivative of the walking motion as a function calculated against observed data, and used this to show the efficacy of the algorithm for walking motion through several applied examples. Analyzing the performance of the proposed algorithm for arbitrary walking motion will yield important information and should be pursued in future work. In addition, we measured real walking motion and determined a realistic walking model. The performance of the proposed method was investigated using this realistic model. The results show that the method can estimate a target shape with good accuracy except at some error points. Performance analysis of the proposed algorithm for arbitrary walking motion including meandering and zigzagging models is an important future task.

References

- [1] A. Lin and H. Ling, "Frontal imaging of human using three-element Doppler and direction-of-arrival radar," *Electron. Lett.*, vol.42, no.11, pp.660–661, 2006.
- [2] A. Lin and H. Ling, "Three-dimensional tracking of humans using very low-complexity radar," *Electron. Lett.*, vol.42, no.18, pp.1062–1063, 2006.
- [3] E.J. Bond, X. Li, S.C. Hagness, and B.D. van Veen, "Microwave imaging via space-time beamforming for early detection of breast cancer," *IEEE Trans. Antennas Propag.*, vol.51, no.8, pp.1690–1705, 2003.
- [4] J. van der Kruk, C.P.A. Wapenaar, J.T. Fokkema, and P.M. van den Berg, "Three-dimensional imaging of multicomponent ground-penetrating radar data," *Geophysics*, vol.68, no.4, pp.1241–1254, 2003.
- [5] T. Sato, T. Wakayama, and K. Takemura, "An imaging algorithm of objects embedded in a glossy dispersive medium for subsurface radar data processing," *IEEE Trans. Geosci. Remote Sens.*, vol.38, no.1, pp.296–303, 2000.
- [6] T. Sakamoto and T. Sato, "A target shape estimation algorithm for pulse radar systems based on boundary scattering transform," *IEICE Trans. Commun.*, vol.E87-B, no.5, pp.1357–1365, May 2004.
- [7] T. Sakamoto and T. Sato, "A phase compensation algorithm for high-resolution pulse radar systems," *IEICE Trans. Commun.*, vol.E87-B, no.11, pp.3314–3321, Nov. 2004.
- [8] T. Sakamoto, "A 2-D image stabilization algorithm for UWB pulse radars with fractional boundary scattering transform," *IEICE Trans. Commun.*, vol.E90-B, no.1, pp.131–139, Jan. 2007.
- [9] T. Sakamoto, "A fast algorithm for 3-dimensional imaging with UWB pulse radar systems," *IEICE Trans. Commun.*, vol.E90-B, no.3, pp.636–644, March 2007.
- [10] T. Sakamoto, H. Matsumoto, and T. Sato, "A high-resolution imaging algorithm for complex-shaped target shapes by optimizing quasi-wavefronts," *Proc. IEEE AP-S International Symposium 2008*, July 2008.
- [11] S. Kidera, T. Sakamoto, and T. Sato, "High-resolution and real-time 3-D imaging algorithm with envelope of spheres for UWB radars," *IEEE Trans. Geosci. Remote Sens.* (inpress).



Takuya Sakamoto was born in Nara, Japan in 1977. Dr. Sakamoto received his B.E. degree from Kyoto University in 2000, and M.I. and Ph.D. degrees from the Graduate School of Informatics, Kyoto University in 2002 and 2005, respectively. He is an assistant professor in the Department of Communications and Computer Engineering, Graduate School of Informatics, Kyoto University. His current research interest is in digital signal processing. He is a member of the IEEJ and the IEEE.



Toru Sato received his B.E., M.E., and Ph.D. degrees in electrical engineering from Kyoto University, Kyoto, Japan in 1976, 1978, and 1982, respectively. He has been with Kyoto University since 1983 and is currently a Professor in the Department of Communications and Computer Engineering, Graduate School of Informatics. His major research interests are system design and signal processing aspects of atmospheric radar, radar remote sensing of the atmosphere, observations of precipitation using radar and satellite signals, radar observation of space debris, and signal processing for subsurface radar signals. Dr. Sato was awarded the Tanakadate Prize in 1986. He is a member of the Society of Geomagnetism and Earth, Planetary and Space Sciences, the Japan Society for Aeronautical and Space Sciences, the Institute of Electrical and Electronics Engineers, and the American Meteorological Society.